Diffractive production of jets and weak bosons and tests of hard-scattering factorization

Lyndon Alvero,[1] John C. Collins,[1] Juan Terron,[2] and J. J. Whitmore[1]

[1]*Physics Department, Pennsylvania State University, 104 Davey Laboratory, University Park, Pennsylvania 16802-6300*
[2]*Universidad Autónoma de Madrid, Departamenta de Física Teórica, Madrid, Spain*

We extract diffractive parton densities from data on diffractive deep inelastic scattering (DIS) and on diffractive photoproduction of jets. We explore the results of several *Ansätze* for the functional form of the parton densities. Then we use the fitted parton densities to predict the diffractive production of jets and of W's and Z's in $p\bar{p}$ collisions at the Fermilab Tevatron. To fit the photoproduction data requires a large gluon density in the Pomeron. The predictions for the Tevatron cross sections are substantially higher than data; this signals a breakdown of hard-scattering factorization in diffractive hadron-hadron collisions.
[S0556-2821(99)00309-4]

PACS number(s): 13.60.Hb, 13.85.Qk, 13.87.−a

I. INTRODUCTION

In view of counterexamples [1,2] to the conjecture of factorization [3] of hard processes in diffractive scattering, it is important to test [4] factorization experimentally. In this paper, we present some results to this end. Specifically, we present fits[1] to data from the ZEUS and H1 Collaborations on diffractive deep inelastic scattering (DIS) [6–8] and on diffractive photoproduction of jets [9]. Then we use these fits to predict cross sections in hard diffractive processes in $p\bar{p}$ collisions, with the assumption of factorization; we find that the predictions fail badly.

We recall that diffractive events are characterized by a large rapidity gap, a region in rapidity where no particles are produced. We are concerned with the case where there is a hard scattering and where the gap occurs between the hard scattering and one of the beam remnants. Such hard diffractive events are observed in DIS experiments [10] and are found to have a large rate: around 10% of the inclusive cross section. Diffractive jet production in $p\bar{p}$ collisions was earlier reported by the UA8 Collaboration [11], but under somewhat different kinematic conditions (larger $|t|$).[2] There was also a report of diffractive bottom production [12]. Now, more diffractive data are being gathered from a variety of lepto-hadronic [6–9] and hadronic [13–18] processes, but with substantially smaller fractions in the case of the diffractive production of jets and weak vector bosons in $p\bar{p}$ interactions than in DIS.

Factorization for diffractive hard scattering is equivalent to the hard-scattering aspects of the Ingelman-Schlein model [3], where diffractive scattering is attributed to the exchange of a Pomeron—a colorless object with vacuum quantum numbers. Ingelman and Schlein treat the Pomeron like a real particle, and so they consider that a diffractive electron-proton collision is due to an electron-Pomeron collision and that a diffractive proton-proton collision is due to a proton-Pomeron collision. Therefore they propose that diffractive hard cross sections are obtained as a product of a hard-scattering coefficient (or Wilson coefficient), a known Pomeron-proton coupling, and parton densities in the Pomeron.

As was already known [2] before the advent of QCD, factorization is not expected to hold in general for diffractive hard processes. Furthermore, on the basis of a breakdown of the triple-Regge theory for soft single-diffractive excitation, Goulianos has proposed [19] to renormalize the Pomeron flux in an energy-dependent way. The agreement between data and his calculated cross sections is evidence that hard-scattering factorization is likely to break down in diffractive hadron-hadron collisions.

However, one of us has recently proved factorization [20] for those diffractive hard processes that are lepton induced: these include diffractive DIS and diffractive *direct* photoproduction of jets. The proof fails for hadron-induced processes. In this formulation, the primary non-perturbative quantities are diffractive parton densities [21–23] in the proton. Although we will use the terminology of "parton densities in the Pomeron," this mainly gives a useful way to describe the kind of parametrization we use for the diffractive parton densities, together with an indication of the quantum numbers that we believe to be exchanged across the rapidity gap. There is no necessary requirement that the object we call the Pomeron be the same as in soft scattering.[3]

In principle, the parton densities in the Pomeron can be extracted from diffractive DIS (F_2) measurements alone. Since the Pomeron is isosinglet and is its own charge conjugate, there is only a single light quark density to measure; one does not have the complication of separating the different flavors of quark that one has in the case of the parton densities of the proton. The Q dependence of the structure functions enables one to determine the gluon density. The H1 Collaboration has already presented [8] a fit of this kind. This type of data sufficiently determines the quark density in the Pomeron, and the H1 fits suggest a large gluon content

---

[1]The fits presented in this paper represent a complete updating of our fits in an earlier report [5].

[2]By t we mean the invariant momentum-transfer-squared from the diffracted hadron.

[3]So Dokshitzer [24] would probably object to our use of the word "Pomeron."

for the Pomeron. However, a more direct measurement of the gluons can be made in photoproduction, since the leading order processes have both quark- and gluon-induced terms. The ZEUS Collaboration has already presented experimental evidence for a large gluon content of the Pomeron; they performed a combined analysis of their results on the diffractive structure function in deep inelastic scattering [6] and on diffractive jet photoproduction [9].

The main result of the ZEUS work was information on the overall normalization of the diffractive parton densities. In this paper, our aim is to obtain more detailed fits including the H1 data, and to use the resulting fits to predict other cross sections. We use data on both DIS and photoproduction. Recently, the ZEUS Collaboration reported [25] new fits to their data that were made independently, but in a similar fashion to ours.

For fitting the DIS data, we use full next-to-leading-order (NLO) calculations. The use of NLO rather than LO calculations is important since the gluon density is larger than the quark density. For the photoproduction data, we use leading-order calculations in a Monte Carlo event generator in order to implement the experimental cuts. The event generator was constructed by two of us [26] as an extension of the POMPYT generator to allow the use of evolved parton densities in the Pomeron. With the resulting diffractive parton densities we calculate hard diffractive processes in hadron-hadron collisions, given the assumption of factorization.

In the past, Ingelman and Schlein [3] and Bruni and Ingelman [27] have made similar calculations for one of the hadron-induced processes that we consider here (W/Z production). Their results have provided a commonly used benchmark in the phenomenology of these processes. They provide a choice of either ''hard'' or ''soft'' distributions of partons in the Pomeron, according to the $\beta \rightarrow 1$ behavior.[4] The hard distributions give larger diffractive cross sections. At that time, there were no data to determine the distributions. We will find that although the quark distributions preferred by the DIS data are hard, our cross sections are substantially below those predicted by Bruni and Ingelman. We will present an analysis of the reasons for the lower values that we find.

Nevertheless, our predictions for hadron-induced cross sections are well above the measurements [13–18], for both W production and jet production. In the case of jet production, the excess only occurs because of the large gluon density that is strongly preferred by the photoproduction data.

This paper is organized as follows. In Sec. II, we show our fits to diffractive deep inelastic and photoproduction data. In Sec. III, we present some details of the formulas used to calculate the cross sections in hadron-hadron processes, and we discuss the kinematics and phase-space cuts that we used. Then in Secs. IV and V, we present and discuss the results obtained for vector boson production and jet production, respectively. Finally, we summarize our findings in Sec. VI.

---

[4]Here, β is the fraction of the Pomeron's momentum that is carried by the struck parton.

Other fits to the diffractive structure functions measured by H1 have been made by Gehrmann and Stirling [28] and by Kunszt and Stirling [21]. Golec-Biernat and Kwieciński [29] assumed a parametrization of the parton densities in the Pomeron and found it to be compatible with the H1 data on diffractive DIS. Their quark densities are about 30% smaller than ours, and they required the momentum sum rule to be valid. The new features of our work are a fit to a wider range of data, including photoproduction, the lack of an assumption of the momentum sum rule, and a calculation of the cross sections for diffractive jet and W and Z production, so as to test factorization by comparison with data from the Collider Defector at Fernilab (CDF) and D0 experiments.

II. PARTONS IN THE POMERON

We will present a series of fits of parton densities in the Pomeron to data on diffractive DIS and diffractive photoproduction of jets. There are four sets of data that we use:

(i) DIS data obtained by ZEUS using the rapidity gap method [6].

(ii) DIS data obtained by ZEUS using their leading proton spectrometer (LPS) [7].

(iii) DIS data obtained by H1 using the rapidity gap method [8].

(iv) Photoproduction data obtained by ZEUS using the rapidity gap method [9].

A. DIS

Diffractive structure functions are related to the differential cross section for the process $e + p \rightarrow e + p + X$:

$$\frac{d^4\sigma_{\text{diff}}}{d\beta dQ^2 dx_{\mathbb{P}} dt} = \frac{2\pi\alpha^2}{\beta Q^4} \{[1 + (1-y)^2] F_2^{D(4)} - y^2 F_L^{D(4)}\},$$

$$(1)$$

where corrections due to Z^0 exchange and due to radiative corrections have been ignored. Here $x_{\mathbb{P}}$ is the fractional momentum loss of the diffracted proton (in the sense of light-cone momentum), and t is the invariant momentum transfer for the diffracted proton. The variables Q^2 and y are the usual DIS variables, and $\beta = x_{\text{Bj}}/x_{\mathbb{P}}$, with x_{Bj} being the usual Bjorken scaling variable of DIS.

Except for the ZEUS LPS data, the momentum transfer t is not measured; so we make fits to the structure function integrated over t, and write the structure function in the form

$$F_2^{D(3)}(\beta, Q^2, x_{\mathbb{P}}) = \int_{-1}^{0} dt \, F_2^{D(4)}(\beta, Q^2, x_{\mathbb{P}}, t). \qquad (2)$$

[We have set the lower limit on t to -1 GeV^2 to avoid including contributions where the putative diffracted proton results from fragmentation of a high p_T jet. This point should not be important at small $x_{\mathbb{P}}$. Moreover, the integrand in Eq. (2) is steeply falling in t so that the contributions to the integral from the region $t < -1$ are quite small.]

We next use hard-scattering factorization, proved in [20], to write the diffractive structure function in terms of diffractive parton densities and hard-scattering coefficients:

$$F_2^{D(3)}(\beta, Q^2, x_{\mathrm{P}}) = \sum_a e_a^2 \beta f_a^{D(3)}(\beta, Q^2, x_{\mathrm{P}})$$

$$+ \text{NLO corrections}, \qquad (3)$$

an equation valid to the leading power in Q. The hard-scattering coefficients are the same as in ordinary inclusive DIS. The predictive power of this equation comes from the Dokshitzer-Gribov-Lipatov-Altarelli-Parisi (DGLAP) evolution equation obeyed by the parton densities and from the universality of the parton densities: they can be used to predict the cross sections for certain other diffractive hard processes. Factorization also holds for the diffractive structure function differential in t.

We now assume that x_{P} is small. It is therefore sensible to use a parametrization of the x_{P} dependence that is motivated by Regge theory.

If Regge factorization is valid, then the dependence on x_{P} is of the form given by Regge theory, and therefore can be represented by a Pomeron flux factor, $f_{\mathrm{P}/p}$, that is related to the Pomeron-proton coupling measured in proton-proton elastic scattering. We do not necessarily expect Regge factorization to be valid. Nevertheless, we will assume that a suitable parametrization of the x_{P}-dependence is of the Regge form, but possibly with different parameters than in proton-proton elastic scattering. If this form is not suitable, then we will find that we cannot fit the data, and a more general parametrization is needed. This can happen even though hard-scattering factorization remains valid in the form, Eq. (3), proved in Ref. [20].

So we will write the diffractive parton densities as a Pomeron flux factor times what are termed parton densities in the Pomeron:

$$f_a^{D(3)}(\beta, Q^2, x_{\mathrm{P}}) = f_{\mathrm{P}/p}(x_{\mathrm{P}}) f_{a/\mathrm{P}}(\beta, Q^2). \qquad (4)$$

Furthermore, we will assume that the Pomeron flux factor is of the Donnachie-Landshoff (DL) [30] form

$$f_{\mathrm{P}/p}^{\mathrm{DL}}(x_{\mathrm{P}}) = \int_{-1}^{0} dt \, \frac{9\beta_0^2}{4\pi^2} \left[\frac{4m_p^2 - 2.8t}{4m_p^2 - t} \left(\frac{1}{1 - t/0.7} \right)^2 \right]^2 x_{\mathrm{P}}^{1 - 2\alpha(t)}, \qquad (5)$$

where m_p is the proton mass, $\beta_0 \simeq 1.8$ GeV^{-1} is the Pomeron-quark coupling and $\alpha(t) = \alpha_{\mathrm{P}} + 0.25t$ is the Pomeron trajectory. We treat α_{P} as a parameter of our fits, instead of using the value given by Donnachie and Landshoff. Up to logarithmic corrections, the flux factor integrated over t is

$$f_{\mathrm{P}/p}(x_{\mathrm{P}}) \simeq C x_{\mathrm{P}}^{1 - 2\alpha_{\mathrm{P}}}, \qquad (6)$$

where C is a constant.

The t-dependence of the DL flux factor is not used in any of our fits; so the only use we make of the t dependence in Eq. (5) is to give a convention for a normalization factor that is convenient for comparisons with other work.

There is in fact another Pomeron flux factor that is commonly used, that of Ingelman and Schlein (IS) [3]. This differs from the DL flux factor primarily in its normalization. Since the same normalization factor appears in all our cross sections, its value is irrelevant to our phenomenology. Any change in the normalization factor is completely compensated for by changing the parton densities by an inverse factor, and we obtain the parton densities from fitting a set of data without any *a priori* expectations as to their normalization.

However, the normalization does affect the question of whether the momentum sum rule is obeyed by the parton densities in the Pomeron. Since it is not at present understood whether the sum rule is a theorem, this issue will not affect us. The momentum sum rule is *not* assumed in any of our fits.

We will use Regge theory to make one further (correctable) assumption; this is, in effect, that the Pomeron has a definite charge conjugation parity and is an isosinglet. This implies that the distributions of u, d, $\bar{u}$ and $\bar{d}$ quarks are equal. Such an assumption is also valid in simple models where the rapidity gap is generated by gluon exchange. One possible mechanism for violation of the equality of the light parton densities would be the existence of an odderon, which has opposite charge conjugation to the Pomeron. The existence of Pomeron-odderon interference would break the equality of the quark and antiquark distributions. We will ignore this possibility, since there is no convincing phenomenological evidence to persuade us of the odderon's existence. We also note that the issue does not concern us in DIS and photoproduction, since the hard-scattering coefficients are the same for quarks and antiquarks; in effect we will measure the average of the quark and antiquark distributions. Odderon contributions would only matter when we make predictions for diffractive cross sections at the Tevatron.

In the data obtained using the rapidity gap method [6,8], the outgoing proton is not detected. Such data include ``double-dissociative'' contributions where the proton is excited to a state that escapes down the beam-pipe and, thus, misses the detector. Factorization works for such final states, but since we will also wish to fit data where the outgoing proton is detected, we prefer to correct the data to remove the double-dissociative contribution. In the case of the ZEUS rapidity gap data [6], excited states up to about 4 GeV pass the diffraction selection cuts, and it is estimated that there is a contribution of $(15 \pm 10)\%$ to the measured diffractive F_2 from double-dissociative events. In obtaining our fits, we have corrected the relevant ZEUS data to take this into account. For the case of photoproduction data, we make the corresponding corrections for double dissociation and for nondiffractive contributions as well. No corrections have been made to the H1 diffractive F_2 data for which excited states up to 1.6 GeV are included. This point is relevant when we compare predictions obtained using our fits to data where the diffracted proton is detected (as in Sec. V) and also when we later compare our fits to both ZEUS and H1 data.

B. Photoproduction of jets

Similar formulas apply to photoproduction. For the direct diffractive photoproduction of a jet, $\gamma + p \rightarrow \text{jet} + X + p$, we let E_T and η be the transverse energy and pseudorapidity of the jet. Then the cross section is

$$\frac{d\sigma}{dx_{\mathrm{P}} dt dE_T d\eta} = \sum_a \int d\beta f_{\mathrm{P}/p}(x_{\mathrm{P}}, t) f_{a/\mathrm{P}}(\beta) \frac{d\hat{\sigma}_{\gamma+a \rightarrow J+X}}{dE_T d\eta}. \tag{7}$$

Here, $d\hat{\sigma}_{\gamma+a \rightarrow J+X}$ is the hard-scattering coefficient for the production of a jet in the collision of a photon and a parton of type a. It is the same as in inclusive photoproduction. The Pomeron flux factor $f_{\mathrm{P}/p}$ and the parton densities in the Pomeron are the same as in the previous section.

The proof [20] of the factorization theorem indicates that factorization is valid for the direct part but probably not for the resolved part of the diffractive photoproduction of jets. Fortunately, most of the cross section is from the direct process. This is known from the experimental data [9], and is also verified by our Monte Carlo calculations. For the kinematic configurations of the data, we find a direct contribution that is 2–4.5 times larger than the resolved contribution, except at $\eta = 0.75$, where the two terms are comparable in size.

If we use the factorization formula to calculate cross sections for diffractive photoproduction, then presumably we should multiply the resolved contribution to the cross section by a correction factor[5] similar to the one needed in hadron-hadron scattering (Secs. IV and V). Given the dominance of the direct contribution and the low precision of the current data—Fig. 3—we feel that this is an unnecessary refinement in the present work.

Beyond leading order, the separation between the resolved and direct processes is not unambiguous. Again, at the level of accuracy of the present data, we think that this is not an important enough issue to affect our results.

C. Selection of data

As far as the DIS data are concerned, we restrict our attention to the subset of the data that is in the truly diffractive region. So we now explain the criteria we use to select the data for our fits.

For the purposes of this paper, we define the diffractive component of a cross section to be the part of the cross section corresponding to the leading-power x_{P}-dependence, of the form in Eq. (6). With this definition of diffraction, the cross sections reported by the ZEUS experiment [6,7,9] are the diffractive components.

We do not need to address the question of whether the power dependence we use, with α_{P} around 1.1 or 1.2, is the

---

[5]On the basis of experimental evidence and of Regge models [2] for diffractive scattering, we might expect the correction factor to be less than unity, a suppression factor. However, the coherent Pomeron mechanism of Collins, Frankfurt and Strikman [1] would enhance the cross section. We will discuss this issue further in the conclusions.

ultimate asymptotic behavior as $x_{\mathrm{P}} \rightarrow 0$. We also do not require that this power be the same as in soft diffraction. It is sufficient that the power law represents an adequate approximation to a measurable part of the cross section, given that the factorization theorem [20] applies quite generally, and not just at small x_{P}. This in fact implies that our restriction to diffractive data is mainly a matter of convenience, to reduce the number of parameters and to be in a region of x_{P} common to the four sets of data to which we make fits.

The H1 data [8] include both non-diffractive and diffractive components, as is evidenced by the experiment's fit to their data with two powers of x_{P}. To restrict our own fit to the diffractive region, we imposed the following cuts on all the DIS data: at $\beta = 0.175$ or 0.2, we require $x_{\mathrm{P}} < 2 \times 10^{-3}$; at $\beta = 0.375$ or 0.4, we require $x_{\mathrm{P}} < 4 \times 10^{-3}$; and at $\beta = 0.65$, we require $x_{\mathrm{P}} < 1 \times 10^{-2}$. We estimated these cuts by examining where the power-law associated with the Pomeron dominates H1's fits to the x_{P} dependence. The H1 data at $\beta = 0.1$ and $\beta = 0.04$ are eliminated from our fits by this criterion.

Another significant constraint is that we must restrict our fits to the truly deep-inelastic region. Outside of this region, the leading-twist QCD factorization theorem for DIS does not hold. In fact some of the H1 data lie very much in the resonance region. For example, they have points at $\beta = 0.9$ and $Q^2 = 4.5$ GeV^2. There the invariant mass of the excited hadronic system is $m_X = Q\sqrt{1/\beta - 1} = 0.7$ GeV, i.e., close to the ρ resonance. While there are perturbative QCD results that apply in this region, they certainly do not include the usual inclusive factorization formula, Eq. (3). Most of H1's data at $\beta = 0.9$ are at low m_X, while the data at smaller β have m_X greater than about 2 GeV. Therefore we have simply chosen to discard the $\beta = 0.9$ data when we make our fits.

With these cuts, the set of data which we fit comprises 77 points, of which 22 are from ZEUS DIS data obtained with the rapidity gap method [6], 3 from ZEUS DIS data from its LPS [7], 48 from H1 DIS data [8], and 4 from the ZEUS photoproduction data [9]. These subsets of data we will call "ZEUS F2D3," "ZEUS LPS," "H1 F2D3," and "ZEUS Photo," respectively.

The region in which we make the fits is shown in Figs. 1, 2 and 3 below, which compare our fits to the data used to make the fits.

D. Fits

Each of our fits is represented by a parametrization of the initial distributions at $Q_0^2 = 4$ GeV^2 for the u, $\bar{u}$, d, and $\bar{d}$ quarks and for the gluon. The other quark distributions are assumed to be zero at this scale. For the DIS cross sections, we used full NLO calculations (with full evolution and with the number of flavors set equal to 3), while for the photoproduction cross sections, we used a version of POMPYT that two of us have constructed [26], with the same evolved parton distributions as we used for DIS. The factorization and renormalization scheme is modified minimal subtraction ($\overline{\text{MS}}$) here and throughout this paper. As stated above, the Pomeron flux factor is of the Donnachie-Landshoff form, Eq. (5), but with an adjustable parameter for α_{P}, and we did not
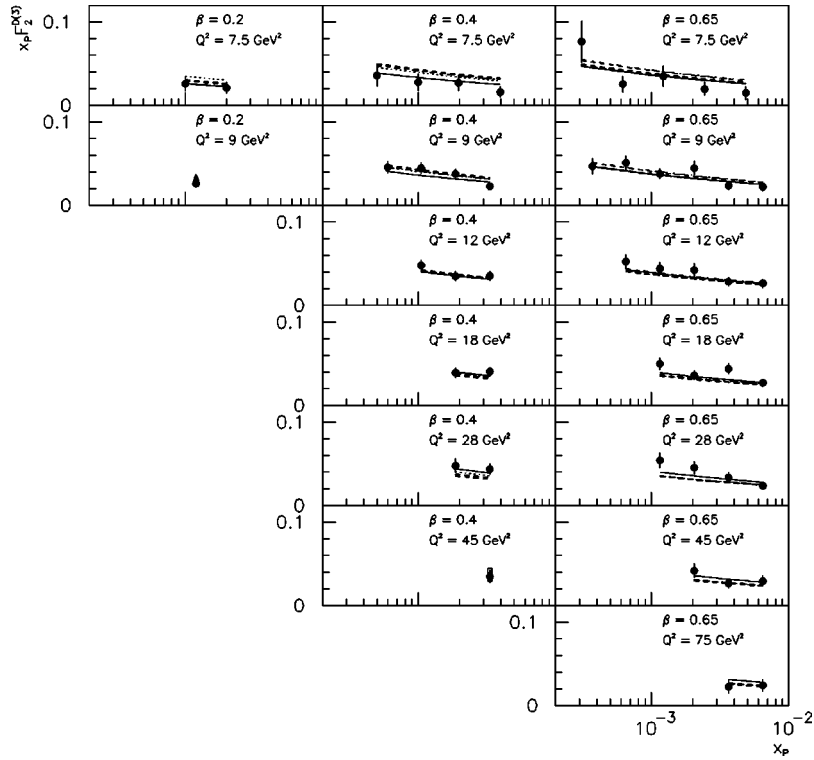
FIG. 1. Comparison of the fits for $\alpha_{\mathrm{P}}=1.14$ and the DIS data from H1 [8] that were used in the fits. Fit A is represented by the dashed line, fit B by the dotted line, fit C by the dot-dashed line, fit D by the solid line, and fit SG by the heavy dashed line.

assume a momentum sum rule for the parton densities in the Pomeron, so that the choice of normalization for the flux factor is irrelevant. The fits were made by minimizing χ^2, with the experimental systematic errors being added in quadrature to the statistical errors; no attempt was made to handle point-to-point correlated errors. The program used to perform the evolution was that of CTEQ [31].

We tried five functional forms for the parton densities, which we label A, B, C, D, and SG. For each of these five forms [Eqs. (8) and (9), below], we present the values of the parameters that give the best fit, given in turn each of the following three values of α_{P}:

(i) $\alpha_{\mathrm{P}}=1.08$, which represents an appropriate value for a conventional Pomeron, as seen in soft scattering.

(ii) $\alpha_{\mathrm{P}}=1.14$, which approximates the best value of α_{P} associated with any of the parametrizations except D.

(iii) $\alpha_{\mathrm{P}}=1.19$, which gives the best fit associated with parametrization D.

Since it is time-consuming to generate Monte Carlo events for the photoproduction process and since the number of photoproduction data is small, we first made some preliminary fits to DIS data alone to determine suitable values for α_{P}, as listed above. Since the χ^2 is not strongly dependent on α_{P}, this seems to us to be sufficient. We will comment on the numerical values later.

Four of the parametrizations, labeled A, B, C and D, use conventional shapes for the initial distributions. The final fit has a gluon distribution that is peaked near $\beta=1$, as suggested by the fit [8] obtained by the H1 Collaboration; we call this our ''super-hard gluon'' SG fit.

Parametrizations A–D are all of the general form

$$\beta f_{q/\mathrm{P}}(\beta,Q_0^2)=a_q[\beta(1-\beta)+\tilde{a}_q(1-\beta)^2],$$

$$\beta f_{g/\mathrm{P}}(\beta,Q_0^2)=a_g\beta(1-\beta), \qquad (8)$$

with a series of constraints on the parameters. Note that since the Pomeron is isosinglet and self-charge-conjugate, the dis-
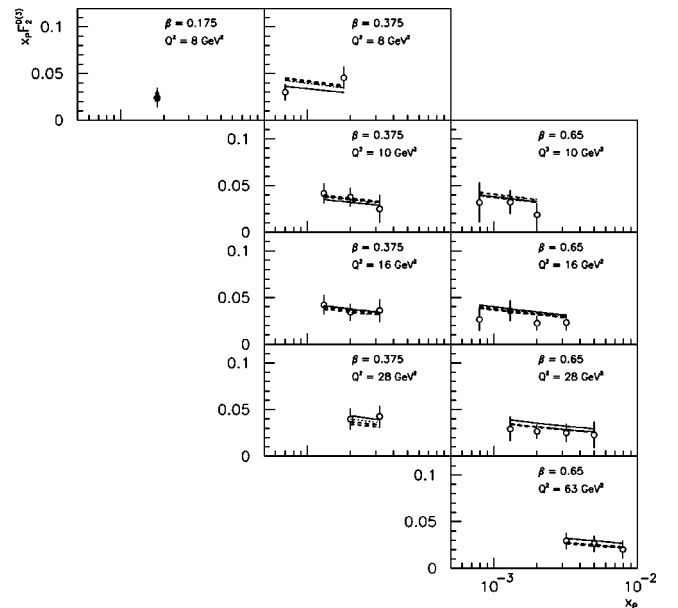

FIG. 2. Comparison of the fits for $\alpha_{\mathrm{P}}=1.14$ and the DIS data from ZEUS [6,7] that were used in the fits. The LPS data we used consist of just the three points at $Q^2=8$ GeV^2. The code for the lines is the same as in Fig. 1.
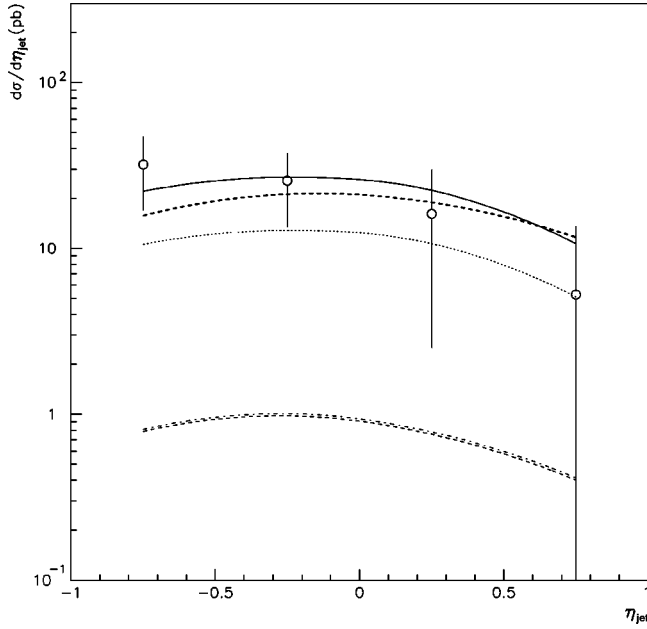
FIG. 3. Comparison of the fits for $\alpha_P = 1.14$ and the ZEUS photoproduction data [9] used in the fits. The code for the lines is the same as in Fig. 1.

tributions of the u, d, $\bar{u}$, and $\bar{d}$ quarks are all equal. Our first parametrization A represents a conventional hard quark parametrization, where we set $\tilde{a}_q = a_g = 0$. Then in parametrization C we allow a soft quark term, while keeping no gluon term, so that $a_g = 0$. In parametrization B we allow an initial gluon distribution but do not allow a soft quark term, so that $\tilde{a}_q = 0$. Finally, in parametrization D we remove all the constraints.

The super-hard gluon parametrization, SG, is of the form

$$\beta f_{q/P}(\beta, Q_0^2) = a_q \beta(1-\beta),$$

$$\beta f_{g/P}(\beta, Q_0^2) = a_g \beta^8 (1-\beta)^{0.3}; \quad (9)$$

i.e., the quark has a hard form, and the gluon is strongly emphasized at large β. The exponents for the gluon distribution were chosen somewhat arbitrarily, with no attempt being made to fit them.

In Table I, we show the parameters for each of the fits, and in Table II we show the values of χ^2, both for the total set of data and for each of the four subsets separately. In Figs. 1 and 2 we compare our fits to the H1 and ZEUS DIS data.

One important property of the fits is that the overall normalization of the quark distribution is quite well determined, as represented by the coefficient a_q. This is not surprising, since the DIS cross section is dominated by a quark-induced process. The systematic shift to lower values of a_q and a_g as α_P increases is entirely due to the fact that the cross section has a factor $1/x_P^{2\alpha_P}$ and that the data are in the region $x_P \lesssim 10^{-2}$.

The next important property is that a large initial gluon distribution is strongly preferred. This can easily be seen

TABLE I. Parameters of the fits for three different values of α_P.

	$\alpha_P = 1.08$		
Fit	a_q	a_g	$\tilde{a}_q$
A	0.496±0.013	0	0
B	0.493±0.013	9.3±2.5	0
C	0.501±0.022	0	−0.008±0.031
D	0.565±0.026	15.4±3.1	−0.113±0.031
SG	0.470±0.015	12.6±3.9	0

	$\alpha_P = 1.14$		
Fit	a_q	a_g	$\tilde{a}_q$
A	0.240±0.006	0	0
B	0.239±0.006	4.5±0.5	0
C	0.249±0.011	0	−0.031±0.029
D	0.292±0.013	9.7±1.7	−0.159±0.029
SG	0.225±0.008	7.4±2.2	0

	$\alpha_P = 1.19$		
Fit	a_q	a_g	$\tilde{a}_q$
A	0.136±0.004	0	0
B	0.135±0.004	2.6±0.6	0
C	0.143±0.006	0	−0.042±0.028
D	0.175±0.008	6.7±1.0	−0.191±0.026
SG	0.126±0.005	5.0±1.4	0

from the comparison to the photoproduction data in Fig. 3. With an initial gluon distribution that is zero, the cross section (dashed or dot-dashed curve) is over an order of magnitude below the data. Even though there are only 4 data points, the improvement when one goes to a parametrization with a large initial gluon distribution is the dominant effect in determining the gluon. The preference is also seen strongly in the χ^2 values for the H1 DIS data—see Table II. However, this preference is also associated with a negative soft-quark term in the initial parton densities, which would appear to be unphysical. We comment on this below.

The relative size of the gluon distributions can be seen in Table III, which gives the momentum sums for the initial parton distributions for each of the fits (in the case that $\alpha_P = 1.14$). Note that the total momentum sum, as opposed to its quark and gluon components, is invariant under DGLAP evolution.

Now let us examine the fits in turn.

Fit A has no gluons and no soft quark term. A good fit to the ZEUS DIS data is obtained: $\chi^2/$(data point) is about 10/22 for the rapidity gap data and 2/3–5/3 for the LPS data (depending on the value of α_P). However, only a moderately good fit is obtained for the H1 data: $\chi^2/$(data point) $\simeq 70/48$. The LPS data show a mild preference for a small value of α_P, but this tendency is overwhelmed in the χ^2 by a strong preference of the H1 data for a larger value: α_P

TABLE II. χ^2 for each of the fits. The data sets and the number of points are ZEUS F2D3, 22 points; ZEUS F2D3 LPS, 3 points; H1 F2D3, 48 points; ZEUS photoproduction, 4 points. The total number of data points is 77.

	$\alpha_P = 1.08$				
Fit	Zeus F2D3	Zeus LPS	H1 F2D3	Zeus Photo	All sets
A	8.2	1.8	81.9	9.9	101.8
B	5.9	2.0	77.7	2.1	87.8
C	8.5	1.8	81.6	9.9	101.8
D	9.3	1.8	65.3	1.2	77.6
SG	6.6	1.9	80.7	2.1	91.2

	$\alpha_P = 1.14$				
Fit	Zeus F2D3	Zeus LPS	H1 F2D3	Zeus Photo	All sets
A	8.6	3.3	68.8	10.1	90.8
B	5.8	3.4	65.3	3.3	77.8
C	9.7	3.2	66.8	10.1	89.7
D	10.8	2.4	42.1	1.1	56.3
SG	6.2	3.7	67.7	1.9	79.6

	$\alpha_P = 1.19$				
Fit	Zeus F2D3	Zeus LPS	H1 F2D3	Zeus Photo	All sets
A	9.5	5.0	72.3	10.2	97.1
B	6.3	4.9	68.3	4.0	83.6
C	11.0	4.7	69.0	10.2	95.0
D	12.4	3.0	34.8	1.0	51.2
SG	6.4	5.8	70.6	2.0	84.9

$=1.14$ gives a much better χ^2 than $\alpha_P = 1.08$. However, the photoproduction data are not reproduced at all.

Fit B differs from fit A by allowing an initial gluon distribution. Not surprisingly, this allows us to fit the photoproduction data much better with the $\chi^2/(\text{data point})$ ranging from 2/4 to 4/4. However, these good χ^2 values are mainly due to the large errors in the last two data points. The Q^2 dependence of the diffractive structure functions, as shown in Fig. 4, illustrates the strong influence of the gluon density on the evolution. We do not get a particularly good fit to the H1 data.

TABLE III. Momentum sums $\int_0^1 d\beta \beta f_{a/P}(\beta)$ at $Q = Q_0 = 2$ GeV for the fits with $\alpha_P = 1.14$. The quark column represents a sum over the 4 light flavors u, d, $\bar{u}$, and $\bar{d}$.

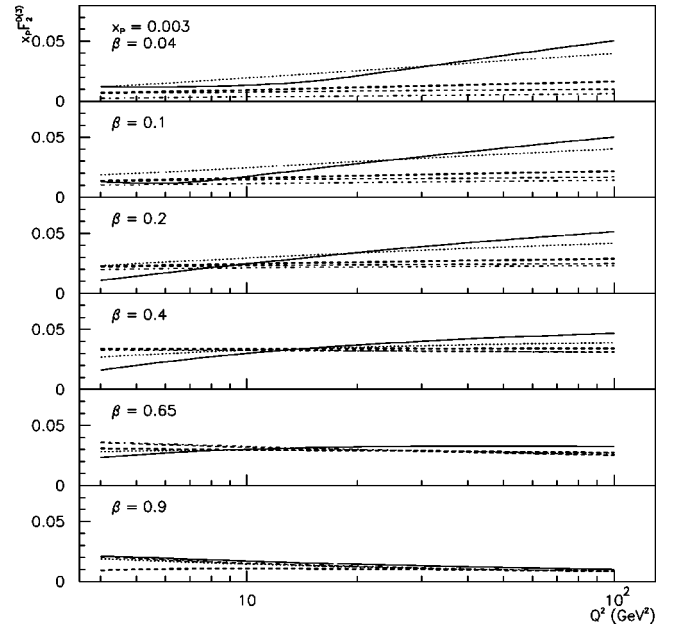| Fit	Quarks	Gluon	Total
A	0.160	0	0.160
B	0.159	0.750	0.909
C	0.156	0	0.156
D	0.133	1.622	1.755
SG	0.150	0.375	0.525

FIG. 4. Q^2 dependence of the fits with $\alpha_P = 1.14$. The code for the lines is the same as in Fig. 1.

We next examine the effect of a soft quark term, in fit D. Although, in general, Regge theory suggests that there should be such a term in the parton densities at some level, what is surprising is that its coefficient is negative. The result is in fact the best of all our fits, including an excellent fit to the photoproduction data. The negative soft-quark term cannot represent the whole story, since it makes the initial quark densities negative at small β. Notice that the quark distribution only becomes negative when β is below the region where we are fitting data, so that we do not have an unphysical quark density. If one wishes to extrapolate our parton densities to low β, it would be sensible to replace the initial quark density by zero whenever the formula gives a negative value. This is in fact done automatically by the CTEQ evolution code that we are using, and one result of this can be seen in Fig. 5. In the curve for fit D at $Q^2 = 4.5$ GeV^2, there is a kink a little below $\beta = 0.2$. Notice that this kink disappears at higher Q^2, when the effects of evolution give a larger positive contribution to the quark density at small β. It is interesting that the restricted set of data to which we fit provides no significant hint of a soft-quark term if we restrict to parton densities with no initial glue—as is seen in fit C.

However, we are not sure to what extent the significance of this estimate of the soft-quark term is to be taken literally. If there were a systematic shift of the data with a series of points moving in a correlated way by about 1 standard deviation, the soft-quark term could be much reduced. Evidence that such a shift is possible is shown in Fig. 6. There we plot DIS data from both experiments. Generally the experiments are compatible, but there is a tendency for the ZEUS data to be about one standard deviation lower than the H1 data for all the plots at $\beta = 0.65$. This would have a significant effect on the χ^2: at the level of ten units, given the number of points.

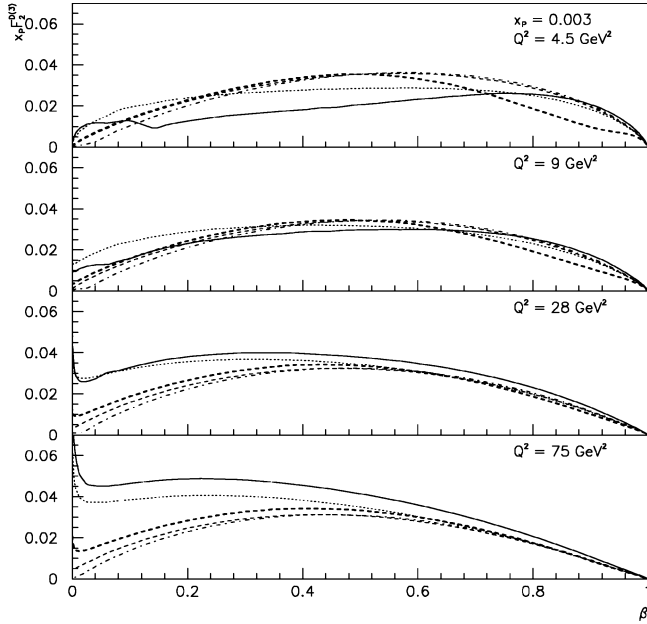Our final fits, SG, have an initial gluon density that is

FIG. 5. β dependence of the fits with $\alpha_P = 1.14$. The code for the lines is the same as in Fig. 1.

peaked at large β, to mimic the one in the fits presented by H1 [8]. Interestingly, we get a good fit to all *but* the H1 data. It should be remembered, however, that we have found it appropriate to fit only to a subset of the data, as explained above, in Sec. II C.

Finally, we comment on the value of α_P. We find that we prefer the value 1.14 for fits A, B, C, and SG. However, fit D gives a value of 1.19. These values are certainly larger than the value for a soft Pomeron, and the lowest χ^2 is given by
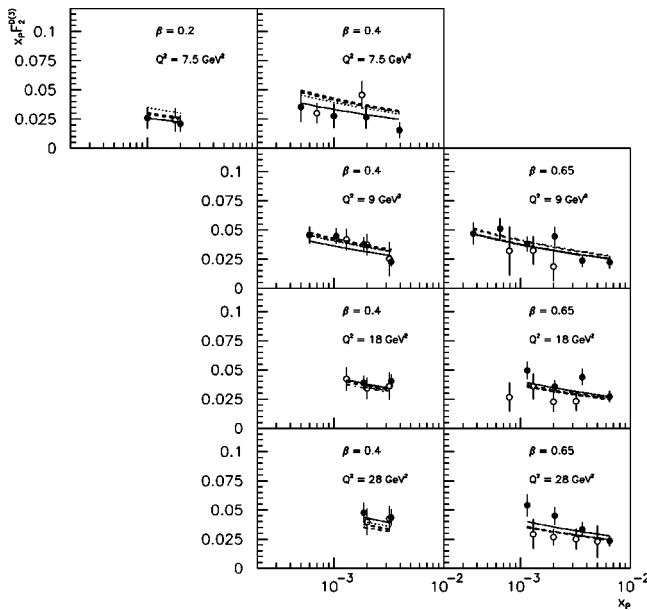

FIG. 6. Comparison of the fits with the DIS data from both the H1 experiment (solid circles) and the ZEUS experiment (open circles), in the region where both experiments have data. The code for the lines is the same as in Fig. 1.

fit D with $\alpha_P = 1.19$, which is compatible with the value preferred by H1 [8]: $\alpha_P = 1.203 \pm 0.020$ (stat) ± 0.013 (syst) $^{+0.030}_{-0.035}$ (model). However, observe that fit D with $\alpha_P = 1.14$ provides a perfectly adequate fit, $\chi^2 = 56.3$ for 73 degrees of freedom, and that the preference for the higher value of α_P is entirely given by the H1 data.

In this context, it is worth examining Fig. 7, where we compare all the H1 data with the predictions of our fits extended beyond the range where we make the fits. Some of the data are in a region of larger x_P where we decided that the cross section is not Pomeron-dominated. The motivation for excluding certain regions of data can be seen particularly clearly in the graphs for $\beta = 0.2$. Furthermore, at $\beta = 0.9$, the data appear to rise more steeply at small x_P than our fits. While this is not conclusive, it suggests that a larger value of the Pomeron intercept, α_P, would be needed to fit this subset of the data. As we explained in Sec. II C, these data are in the resonance region and it is thus not correct to include them in our fitting or to apply the factorization theorem in this region.

Moreover, it has been established that the Pomeron trajectory is not universal, since the value of α_P in hard scattering is not the same as in soft scattering. The proof of factorization certainly does not require such universality. Therefore, there is no reason to assume that the same value of α_P applies to exclusive deep-inelastic processes and to the normal DIS region to which the factorization formula applies.

Factorization does apply two constraints, however. First, parton densities are universal within the class of processes to which the factorization theorem applies; α_P must be the same in these different processes. The second constraint arises from DGLAP evolution. Since evolution relates parton densities at different values of Q and β, variations of α_P with β and Q cannot be totally arbitrary. For example, suppose that at some particular value of Q, the value of α_P were larger at large β than at small β. Then evolution to larger Q would make the largest value of α_P dominate at all β.

E. Shape of diffractive parton densities

Since there are DIS data for a range of values of β, the data do provide information on the shape of the diffractive quark distribution. For example, we are able to obtain significant information on the soft quark parameter $\tilde{a}_q$ in Eq. (8).

However, we do not yet have similar information on the shape of the diffractive gluon distribution. We have two fits D and SG that provide good fits to the photoproduction data, but with dramatically different shapes. A direct measurement of the shape of the diffractive gluon distribution can be made in diffractive photoproduction of dijets by using the cross section $d\sigma/d\beta^{\text{OBS}}$, where β^{OBS} is the longitudinal (light-front) momentum of the jet pair relative to the Pomeron. In the leading-order parton approximation, β^{OBS} is exactly the momentum fraction of the parton in the Pomeron initiating the hard scattering.

We see the implications of these observations in Fig. 8, where we superimpose our predictions on preliminary data [25] for the diffractive photoproduction of dijets as a func-
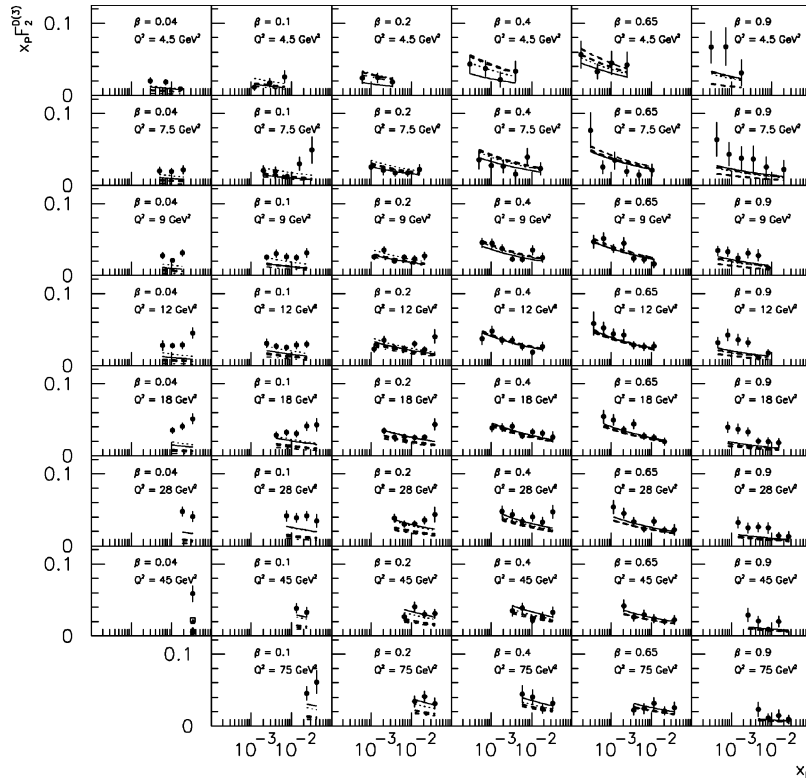
FIG. 7. Comparison of the fits for $\alpha_P = 1.14$ and all the DIS data from H1 [8]. The code for the lines is the same as in Fig. 1.

tion of each of several kinematic variables. The only plot that enables us to distinguish the D and SG fits is that of the β^{OBS} dependence. The singular gluon is evidently preferred. In the other plots, both D and SG reproduce the normalization and shape of the cross section.
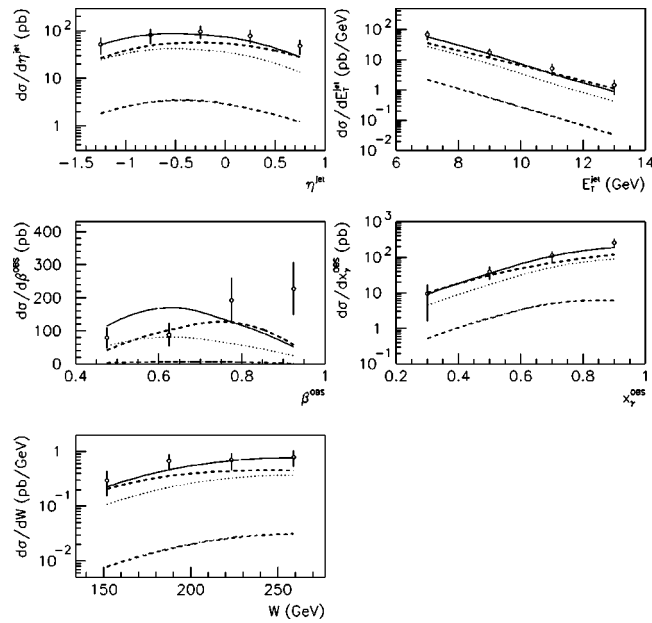

FIG. 8. Comparison of the fits for $\alpha_P = 1.14$ and the preliminary 1994 ZEUS photoproduction data [25]. The code for the lines is the same as in Fig. 1. A double dissociation contribution of (31 $\pm 13)\%$ has been subtracted from the data. Note that these data were not used in the fits.

In this same paper [25], fits of diffractive parton densities were presented. These were made independently of ours, with the same kinds of parametrization, but with the inclusion of only the ZEUS data; the results, particularly as regards the gluon distribution, are in general agreement with ours.

The preference for a singular gluon distribution is in agreement with the H1 conclusions [8]. It is interesting that in our fits the subset of the H1 data that we use shows the opposite preference—see Table II.

III. KINEMATICS AND CROSS SECTIONS FOR HADRON-INDUCED PROCESSES

We now consider the production of W and Z bosons and of jets in diffractive $p\bar{p}$ collisions. In addition, we consider W production with explicit measurement of the distribution of the final-state leptons. Schematically, these processes are

$$p(p_1) + \bar{p}(p_2) \rightarrow (W \text{ or } Z) + \bar{p} + X,$$

$$p(p_1) + \bar{p}(p_2) \rightarrow \text{jet} + \bar{p} + X,$$

$$p(p_1) + \bar{p}(p_2) \rightarrow (W \rightarrow l + \nu) + \bar{p} + X. \tag{10}$$

We take the Pomeron to be emitted from the antiproton and the positive z-axis to be along the antiproton's direction.

A. Diffractive jet production

Consider the diffractive cross section for the production of a jet with rapidity y, in a hadron-hadron collision. We will assume hard-scattering factorization [3,4]. At leading order, the hard-scattering process is $2 \rightarrow 2$ at the parton level, and results in a cross section of the form

$$
\frac{d\sigma^{\mathrm{jet}}}{dy} = \sum_{a,b} \int dE_T \, 2E_T \int dy' \int dx_{\mathbb{P}} f_{\mathbb{P}/\bar{p}}(x_{\mathbb{P}}, \mu)
$$

$$
\times f_{a/p}(x_a, \mu) f_{b/\mathbb{P}}(x_b, \mu) x_a x_b \frac{d\hat{\sigma}^{\mathrm{jet}}_{ab}}{d\hat{t}}, \qquad (11)
$$

where the sum is over all the active parton (quark, antiquark and gluon) flavors. The integration variables are E_T, the transverse energy of the jet, y', the rapidity of the other jet, and $x_{\mathbb{P}}$, the momentum fraction of the Pomeron. The momentum fractions of the partons, relative to their parent proton and Pomeron are

$$
x_a = \frac{E_T}{\sqrt{s}}(e^{-y} + e^{-y'}) \quad \text{and} \quad x_b = \frac{E_T}{\sqrt{s}x_{\mathbb{P}}}(e^{y} + e^{y'}).
$$
$$
(12)
$$

The functions $f_{a/p}(x_a)$ and $f_{b/\mathbb{P}}(x_b)$ are the number densities of partons in the proton and Pomeron, respectively, while $f_{\mathbb{P}/\bar{p}}$ is the same Pomeron flux factor that we used in Sec. II A [see Eq. (5)]. $d\hat{\sigma}^{\mathrm{jet}}_{ab}/d\hat{t}$ is the partonic hard-scattering coefficient, and μ is the factorization scale, which we set equal to E_T. The limits on the integrations are determined by the experimental conditions.

The diffractive cross section given by Eq. (11) has the same structure as the factorized form of the corresponding inclusive cross section (i.e., without the diffractive requirement), except for the Pomeron flux factor and the parton densities in the Pomeron. The same hard-scattering coefficient and nucleon parton distribution functions appear in both cross sections.

The cross section given by Eq. (11) has contributions from a range of subprocesses. The indices a,b labeling the incoming partons range over the gluon and all the flavors of quarks and antiquarks. The LO form of the partonic cross section $d\hat{\sigma}^{\mathrm{jet}}_{ab}/d\hat{t}$ may be found in [32].

B. Diffractive W and Z production

The cross section for the diffractive production of weak vector bosons is given by

$$
\sigma^{VB} = \sigma^{VB}_0 \sum_{a,b} \int \frac{dx_{\mathbb{P}}}{x_{\mathbb{P}}} \int \frac{dx_b}{x_b} \int \frac{dx_a}{x_a} f_{\mathbb{P}/\bar{p}}(x_{\mathbb{P}}) f_{b/\mathbb{P}}(x_b)
$$

$$
\times f_{a/p}(x_a) \, \tilde{C}^{VB}_{ab} \, \omega_{ab}\left(\frac{\tau}{x_a x_b x_{\mathbb{P}}}, \alpha_s\right), \qquad (13)
$$

where $\sigma^{VB}_0 = \sqrt{2}\pi G_F M^2_{VB}/3s$, $M_{VB} = M_W$ or M_Z is the vector boson mass, G_F is the Fermi constant, x_b, x_a are momentum fractions of partons from the Pomeron and proton, re-

spectively, and $\tau = M^2_{VB}/s$. For W bosons, $\tilde{C}^W_{qq'} = |V_{qq'}|^2$ if $e_q + e_{q'} = \pm 1$ and zero otherwise, where q denotes a quark flavor, e_q the fractional charge of quark q and $V_{qq'}$ is the Cabibbo-Kobayashi-Maskawa matrix element. For Z bosons, $\tilde{C}^Z_{q\bar{q}} = 1/2 - 2|e_q|\sin^2\theta_W + 4|e_q|^2\sin^4\theta_W$, where θ_W is the Weinberg or weak-mixing angle. Similar expressions apply for $\tilde{C}^W_{qg}$ and $\tilde{C}^Z_{qg}$ which are relevant for gluon-induced scattering. The hard-scattering function ω_{ab} in the $\overline{\mathrm{MS}}$ scheme and to NLO in the QCD strong coupling α_s can be found in [33].

C. Diffractive production of leptons from the W

Since leptonic decays of W bosons include an unobserved neutrino, it is useful to compute the distribution of the observed charged lepton. The general formula for the distribution of leptons from W production has the same form as that for jet production, Eq. (11). In this case, we are only going to compute cross sections at leading order. Data have not been published for this particular cross section, but since it is directly measurable, we think it is a useful quantity to work with.

For the specific process $p + \bar{p} \rightarrow (W^- \rightarrow e + \bar{\nu}_e) + \bar{p} + X$, we have the leading-order cross section for quark-antiquark annihilation to a lepton pair:

$$
\frac{d\hat{\sigma}^{\mathrm{lep}}_{ab}}{d\hat{t}} \simeq \frac{G^2_F}{6M_W\Gamma_W} \tilde{C}^W_{ab} \, \delta(x_a x_b s - M^2_W) \, \hat{u}^2, \qquad (14)
$$

where Γ_W is the width of the W boson and $\hat{u} = -x_b x_{\mathbb{P}} \sqrt{s} E_T e^{-y}$. Using Eq. (14) in Eq. (11), one obtains the following cross section at the hadronic level:

$$
\frac{d\sigma^{\mathrm{lep}}}{dy} = \sum_{a,b} \int \frac{dx_{\mathbb{P}}}{x_{\mathbb{P}}} \int dE_T f_{\mathbb{P}/\bar{p}}(x_{\mathbb{P}}) f_{b/\mathbb{P}}(x_b) f_{a/p}(x_a) \tilde{C}^W_{ab}
$$

$$
\times \left[\frac{\hat{u}^2 G^2_F}{6s\Gamma_W[(M_W/2E_T)^2 - 1]^{1/2}} \right], \qquad (15)
$$

where x_a and x_b are now given by

$$
x_a = \frac{M_W e^{-y}}{\sqrt{s}} \left[\frac{M_W}{2E_T} + \sqrt{\left(\frac{M_W}{2E_T}\right)^2 - 1} \right],
$$

$$
x_b = \frac{M^2_W}{s} \frac{1}{x_a x_{\mathbb{P}}}. \qquad (16)
$$

We have suppressed the scale dependence of the functions $f_{i/j}$ in Eqs. (13) and (15); in actual computations, we set the scale equal to the vector boson mass. A similar equation may be obtained for the W^+ cross section.

D. Inclusive cross sections

Since we are particularly interested in the percentage of events that are diffractive, we also need to calculate the inclusive cross sections, that is, the ones without the diffractive

requirement on the final state. The analogue to Eq. (11) for the inclusive cross section for jet production is the standard formula

$$\frac{d\sigma^{\text{jet, incl}}}{dy} = \sum_{a,b} \int dE_T 2E_T \int dy' f_{a/p}(x_a,\mu)$$

$$\times f_{b/\bar{p}}(x_b,\mu)x_a x_b \frac{d\hat{\sigma}^{\text{jet}}_{ab}}{d\hat{t}}, \quad (17)$$

where x_a is given in Eq. (12), while x_b is now $x_b = (e^y + e^{y'})E_T/\sqrt{s}$.

For the leptons from W^- production, the inclusive version of Eq. (15) is

$$\frac{d\sigma^{\text{lep, incl}}}{dy} = \sum_{a,b} \int dE_T f_{b/\bar{p}}(x_b,\mu) f_{a/p}(x_a,\mu) \, \tilde{C}^W_{ab}$$

$$\times \left[\frac{\hat{u}^2 G_F^2}{6s\Gamma_W[(M_W/2E_T)^2-1]^{1/2}} \right], \quad (18)$$

with a similar equation for W^+ production. In Eq. (18), $\hat{u} = -x_b\sqrt{s}E_T e^{-y}$, x_a is as defined in Eq. (16) while x_b is now given by $x_b = M_W^2/x_a s$.

The analogue to Eq. (13) for the inclusive total cross section for vector boson production is

$$\sigma^{\text{VB}} = \sigma_0^{\text{VB}} \sum_{a,b} \int \frac{dx_a}{x_a} \int \frac{dx_b}{x_b} f_{a/p}(x_a) f_{b/\bar{p}}(x_b) \, \tilde{C}^{\text{VB}}_{ab}$$

$$\times \omega_{ab}\left(\frac{\tau}{x_a x_b}, \alpha_s \right). \quad (19)$$

IV. NUMERICAL CALCULATIONS OF W AND Z PRODUCTION

For the calculations in this section, the factorization scale in the parton distributions was set to M_{VB}. The values of the electroweak parameters that appear in the various formulas were taken from Ref. [34], and we use only four flavors (u,d,s,c) in the weak mixing matrix, with the Cabibbo angle $\theta_C = 0.2269$.

A. Comparison with previous calculations

Bruni and Ingelman [27] computed diffractive W/Z cross sections neglecting any Q^2 evolution of the parton distributions in the Pomeron. At $\sqrt{s} = 1800$ GeV, they obtained the following diffractive fractions $(R = \sigma^{\text{diff}}/\sigma^{\text{incl}})$: $R_{W^+ + W^-} \simeq 20\%$ and $R_Z \simeq 17\%$ for total W and Z production, respectively. These rates are substantially larger than the few percent measured by CDF in [13].

As we will now explain, when one uses evolved Pomeron parton densities from our fits to data from the DES ep colleder HERA, one obtains substantially smaller rates than the Bruni-Ingelman ones. To understand these small rates, we first verify that we can reproduce the Bruni-Ingelman results. For these, we used their unevolved hard quark distribution in

TABLE IV. Inclusive cross sections $\sigma^{W,Z\,\text{incl}}$ (pb) for weak vector boson production.

	EHLQ1 Ref. [27] LO	EHLQ1 LO	EHLQ1 NLO	CTEQ4M LO	CTEQ4M NLO
$W^+ + W^-$	14000	14300	18100	18700	23500
Z	4400	4400	5600	5500	6900

the Pomeron [given by their Eq. (4)], the same cut on $x_{\mathbb{P}} : x_{\mathbb{P}}^{\max} = 0.1$, the Eichten-Hinchliffe-Lane-Quigg set 1 (EHLQ1) parton distributions in the proton and the IS flux factor:[6]

$$f^{\text{IS}}_{\mathbb{P}/p}(x_{\mathbb{P}}) = \int dt \frac{1}{2.3 x_{\mathbb{P}}} (3.19 e^{8t} + 0.212 e^{3t}). \quad (20)$$

The flux in Eq. (20) differs by a factor of 1/2 from that in [27] because here we consider the case when only $\bar{p}$ diffracts while [27] considers the case when either p or $\bar{p}$ diffracts.

Next, we evolved their Pomeron parton distributions and recalculated the cross sections. Finally, to provide our best estimates of the rates, we repeated the calculations using CTEQ4M for the parton densities in the proton or antiproton and using our fits for the parton densities in the Pomeron, all with proper evolution. The cross sections were calculated using Eqs. (13) and (19) and the results obtained are summarized in Tables IV–VI.

First, in Table IV, we show the *inclusive* cross section, σ^{incl}, which will give the denominator for the fraction of the cross section that is diffractive. We present the LO result from [27] as well as our leading and NLO results. At leading order, one observes that the use of the more up-to-date CTEQ4M densities in the proton instead of the EHLQ1 densities used by Bruni and Ingelman leads to cross sections that are 20%–30% higher. Including the next-to-leading order contributions leads to another similar increase in the cross sections.

The diffractive cross sections $\sigma^{W,Z\,\text{diff}}$ are shown in Tables V and VI. In the columns labeled ''BI,'' we used the Bruni-Ingelman parton density in the Pomeron and the EHLQ1 parton densities in the proton, together with the Ingelman-Schlein flux factor (20). In the other columns we used our fits for the parton densities in the Pomeron together with the CTEQ4M parton distributions in the proton; we use the Donnachie-Landshoff form for the flux factor, Eq. (5), and $\alpha_{\mathbb{P}} = 1.14$. First, we use the same cut $x_{\mathbb{P}}^{\max} = 0.1$ as was used by Bruni and Ingelman to produce Table V. However, this allows $x_{\mathbb{P}}$ to be rather larger than where Pomeron exchange is expected to dominate. So we also made calculations with $x_{\mathbb{P}}^{\max} = 0.01$, for which the results are shown in Table VI.

---

[6]Note that since our purpose in using the IS flux is to compare our results with the Bruni-Ingelman calculations, we have used a Pomeron intercept of unity instead of the more accurate value used in our fits.

TABLE V. Diffractive cross section $\sigma^{W,Z\,\mathrm{diff}}$ (pb) for weak vector boson production when only $\bar{p}$ diffracts and with $x_\mathrm{P}^{\max}=0.1$. The cross sections using the BI distributions were computed with $\alpha_\mathrm{P}=1$, as in Ref. [27], but the cross sections using fits A and D were computed with $\alpha_\mathrm{P}=1.14$.

Pomeron:	BI [27] Unevolved	BI Unevolved		BI Evolved		Fit A Evolved		Fit D Evolved	
Proton:	EHLQ1	EHLQ1		EHLQ1		CTEQ4M		CTEQ4M	
	LO	LO	NLO	LO	NLO	LO	NLO	LO	NLO
$W^+ + W^-$	1400	1400	1800	1000	1300	300	390	650	810
Z	380	380	480	260	330	77	100	170	210

In column 3 of Table V we show our leading order results when we use the same unevolved parton densities as Bruni and Ingelman; we agree with their cross sections (column 2). Then we repeat the calculations but with correctly evolved parton densities in the Pomeron, with the Bruni-Ingelman formula being used as the initial data for the evolution at $Q_0^2=4$ GeV^2 (column 5). The corresponding next-to-leading order cross sections are shown in columns 4 and 6. We see that at either LO or NLO, evolution of the Pomeron parton densities leads to about a 30% reduction in the cross section.

We also present in Table VII the diffractive fractions for total W production when either p or $\bar{p}$ diffracts. The fractions are obtained by dividing twice the diffractive cross sections in Tables V and VI (which are for *single-sided* diffraction) by the appropriate inclusive cross section in Table IV.

The diffractive fraction obtained from the evolved BI Pomeron parton distribution, using columns 3 and 4 of Table IV for $\sigma^{W,Z\,\mathrm{incl}}$, is about 14% for W production, compared with the 20% that is obtained using the unevolved BI Pomeron distributions. The corresponding percentages for Z production are a little smaller: 12% (evolved) and 17% (unevolved).

In the last four columns of Tables V and VI we present the results when two of our fits (with $\alpha_\mathrm{P}=1.14$) shown in Sec. II are used. Fit A is the one with a simple hard quark distribution and no glue as the initial values, while fit D, which has both quarks and gluons initially, is our best fit overall. Now fit A does not have the large gluon content that is necessary to fit the photoproduction data; so cross sections computed using fit A cannot be said to represent good predictions. However, it is adjusted to fit DIS data, so that a

TABLE VI. Diffractive cross section $\sigma^{W,Z\,\mathrm{diff}}$ (pb) for weak vector boson production when only $\bar{p}$ diffracts, but now with $x_\mathrm{P}^{\max}=0.01$. The cross sections using the BI distributions were computed with $\alpha_\mathrm{P}=1$, as in Ref. [27], but the cross sections using fits A and D were computed with $\alpha_\mathrm{P}=1.14$.

Pomeron:	BI Evolved		Fit A Evolved		Fit D Evolved	
Proton:	EHLQ1		CTEQ4M		CTEQ4M	
	LO	NLO	LO	NLO	LO	NLO
$W^+ + W^-$	25	38	9	14	14	21
Z	3.2	5.0	1.1	1.8	1.6	2.5

comparison of predictions using fits A and D pinpoints situations where the large gluon distribution has a large effect.

We have also calculated the cross sections resulting when we use the versions of the diffractive parton densities with a higher value of the Pomeron intercept, $\alpha_\mathrm{P}=1.19$. We find that the cross sections are reduced by 10%–20%, depending on the value of $x_\mathrm{P}^{\max}$. The reduced cross section arises because the diffractive parton densities are constrained to fit ZEUS and H1 data at fairly small values of x_P and we are now calculating cross sections at higher values of x_P. So an increase in α_P results in a decrease in our calculated cross section for the hadron-induced processes.

The LO and NLO cross sections resulting from fit A (columns 7 and 8 of Table V) are only about 30% of the evolved BI cross sections. (We will indicate the sources of this difference below, in Sec. IV B.) The diffractive fractions obtained from this fit, using the CTEQ4M entries in Table IV, are 3.3% (2.9%) for $W(Z)$ production, as shown in Table VII.

The quark distributions in fit D are about 20% higher than in fit A—see the values of a_q in Table I. However, the cross sections for W production with fit D exceed those with fit A by a substantially larger factor, particularly at $x_\mathrm{P}^{\max}=0.1$, where the cross section is more than a factor of 2 higher. This arises because of evolution: the large gluon distribution in fit D increases the quark distribution at $\mu=M_W$ compared with the case without the large gluon distribution. The increased quark density is most pronounced at small fractional momentum. Thus the effect is larger at $x_\mathrm{P}^{\max}=0.1$ than at $x_\mathrm{P}^{\max}=0.01$, since in the first case, the quark from the Pomeron that makes the W has a smaller fractional momentum relative to the Pomeron. The NLO contributions further increase the fit D cross sections by 24%. Even so, the cross sections are still smaller, by a factor of 1.6, than the ones from evolved BI Pomeron parton distributions. The rates from fit D (using NLO values) are 6.9% (6.1%) for $W(Z)$ production. These rates agree with those obtained by Kunszt and Stirling [21] with their model 2 for diffractive parton distributions.

The data from which our fits were extracted used a conservative cut on the Pomeron momentum, $x_\mathrm{P}^{\max}=0.01$. The Pomeron flux factor allows for the x_P dependence, but to ensure maximum compatibility with the HERA data without the assumption of standard Regge behavior, the same cut should be applied to the cross sections in hadron-hadron collisions. This results in the cross sections in Table VI, which

TABLE VII. Diffractive fractions using NLO cross sections for $W^+ + W^-$ and Z production when either p or $\bar{p}$ diffracts.

	BI (unevolved) $x_{\mathrm{P}}^{\max}=0.1$	Fit A $x_{\mathrm{P}}^{\max}=0.1$	Fit D $x_{\mathrm{P}}^{\max}=0.1$	Fit A $x_{\mathrm{P}}^{\max}=0.01$	Fit D $x_{\mathrm{P}}^{\max}=0.01$
$W^+ + W^-$	20%	3.3%	6.9%	0.12%	0.18%
Z	17%	2.9%	6.1%	0.05%	0.07%

therefore represent our most accurate prediction of diffractive W and Z production, given only the assumption of hard-scattering factorization, *which of course we wish to test*. Notice that with this cut the diffractive cross sections are over an order of magnitude smaller than with $x_{\mathrm{P}}^{\max}=0.1$. The percentages obtained with this cut on x_{P} for $W(Z)$ production are 0.12% (0.05%) and 0.18% (0.07%) using fits A and D, respectively, as shown in Table VII. The large reduction is due to the fact that we are not far from an effective kinematic limit: the cut on x_{P} gives a maximum proton-Pomeron energy of 180 GeV, and partons typically do not carry the whole of the energy of their parent hadrons.

B. Why are the fractions smaller than from BI?

Although the data used in our fits support a "hard" quark distribution in the Pomeron, we predict that the diffractive W and Z cross sections are much smaller than those predicted by Bruni and Ingelman, who also used hard quark distributions. For example, the diffractive fraction for W production computed using fit A is 6 times smaller than Bruni and Ingelman's fraction (see Table VII).

Since Bruni and Ingelman's work served as an initial benchmark for subsequent work, it is interesting to understand the sources of this factor. We first address fit A, since that is our parametrization that is closest to Bruni and Ingelman's. The factor between the diffractive rates arises as an accumulation of several modest factors:

(i) A factor of 0.9 because of the use of the CTEQ4M instead of the obsolete EHLQ1 distributions in the proton. (The denominator in the ratio of diffractive to inclusive cross sections increases by more than the numerator.)

(ii) A factor of 0.7 for the effect of the evolution of the parton densities in the Pomeron.

(iii) A factor of 1.7 for the use of the Donnachie-Landshoff flux factor instead of the Ingelman-Schlein flux factor, when the momentum sum is kept fixed. We have found that this factor arises from the following:

(a) A factor of 2.5 to allow for our larger value of α_{P}.

(b) A factor of 0.7 to allow for the effects of the Pomeron slope α'.

(iv) A factor of 0.16 because the DIS data indicate that the quarks have a momentum sum substantially less than the value of unity that was assumed by Bruni and Ingelman.[7]

_____

[7] Note that in the case of the diffractive DIS cross section, this small momentum sum is mostly compensated by the effects of our larger value of α_{P}, which increases the cross sections at small x_{P}.

The first three factors in fact cancel. So one possible view is that the smallness of our results compared with those of Bruni and Ingelman arises essentially because of the change in the momentum sum of the quarks required by a fit to the data. An alternative view arises when one observes that the Pomeron-proton coupling is obtained by fitting data on high energy scattering, and that if one increases α_{P}, then the value of the Pomeron-proton coupling has to be decreased to keep the cross section at some particular energy fixed. (Of course, the energy dependence of the cross section would not be fitted so well.) The variable in high-energy scattering that corresponds to $1/x_{\mathrm{P}}$ for hard diffraction is s/M^2. Now, the typical value of x_{P} in the data that we fit is about 10^{-3}, which corresponds to $s \sim 1000$ GeV^2, i.e., a fixed target energy of around 500 GeV. Therefore it is possible to argue that the factor of 2.5 for the larger value of α_{P} should be combined with the factor of 0.16 for the momentum sum, to produce a factor of 0.4 for the momentum sum with the Pomeron-proton coupling fixed at a value appropriate for fixed-target CERN and Fermilab experiments. The overall reduction in our rates compared with those of Bruni and Ingelman then arises as a product of several factors, all less than unity.

The effects of this decrease in cross section in going from the Bruni-Ingelman *Ansatz* to our fitted distribution A are then somewhat compensated by the effects of the large gluon distribution we find in fit D.

C. Lepton distributions for W production at the Tevatron

In this section, we present our results for W production, but now with cuts on the emitted lepton l. Specifically, we calculate the electron's (or positron's) rapidity (y) distribution from Eq. (15) for the diffractive process and from Eq. (18) for the inclusive one. For the parton distributions in the Pomeron, we use our five fits with $\alpha_{\mathrm{P}}=1.14$—see Eqs. (8), (9) and Table I—evolved up to the W mass. We imposed a cut of 20 GeV on the E_T of the emitted lepton, and we integrated x_{P} up to $x_{\mathrm{P}}^{\max}=0.01$.

Figure 9 shows our results for W^- production. For comparison, we also show the inclusive cross section rescaled by 5×10^{-4} as represented by the lower dotted curve. The diffractive cross sections exhibit a strong falloff in the region $y_e > -0.2$ that is a consequence of the requirement of a rapidity gap. This falloff is of course not present in the inclusive cross section.

The diffractive cross sections are about 2%–4% of the inclusive one at the left edge of the plots (at $y = -3$) depending on the fit used. At about $y = -1.6$ where the diffrac-
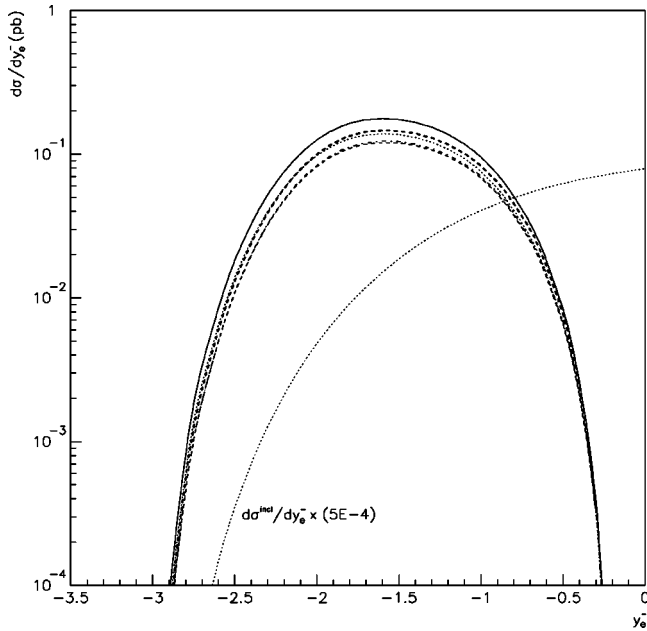
FIG. 9. Rapidity distribution of e^- in W^- production with the cut $x_P < 0.01$. The solid curve results from using fit D, upper dashed curve with fit SG, dotted curve with fit B, lower dashed curve with fit A and dot-dashed curve with fit C. The lower dotted curve is the inclusive cross section scaled down by a factor of 5×10^{-4}.

tive cross sections peak, this fraction drops to about 0.4% –0.6% of the inclusive cross section. The cross sections using high glue fits D, B and SG, denoted by solid, dotted and upper dashed curves, respectively, are larger (D gives largest cross section) than those using the low glue fits A (dashed) and C (dot-dashed) which overlap in the figure. The differences between the cross sections reflect first the size of the quark densities and then, in fits B, D and SG, the effects of a large gluon distribution on the evolution of the quark distribution. For example, fit SG has a smaller quark distribution than fit A, but its large gluon distribution pulls the cross section above that given by fit A. However, the differences are moderate, at most a factor of 1.5.

The corresponding cross sections for W^+ are shown in Fig. 10. The cross sections are larger than for the W^-, because a valence up quark from the proton can be used to make a W^+, especially at large negative rapidities. In the plot, the rapidity gap exists for $y_{e^+} > -1.6$. The same features as in the curves of Fig. 9 can be observed and, thus, the same general inferences for W^- production can be made for this case as well.

D. Comparison to CDF data for W production

The CDF Collaboration has presented data on diffractive W production from $p\bar{p}$ collisions at $\sqrt{s} = 1800$ GeV [13]. The W's are produced with a rapidity gap in the region $2.4 < |\eta| < 4.2$. They find that the fraction of diffractive to non-diffractive W production is [13] $R_W = [1.15 \pm 0.51(\text{stat}) \pm 0.20(\text{syst})]\%$. This value corresponds to diffractive data corrected up to $x_P = 0.1$ [35].
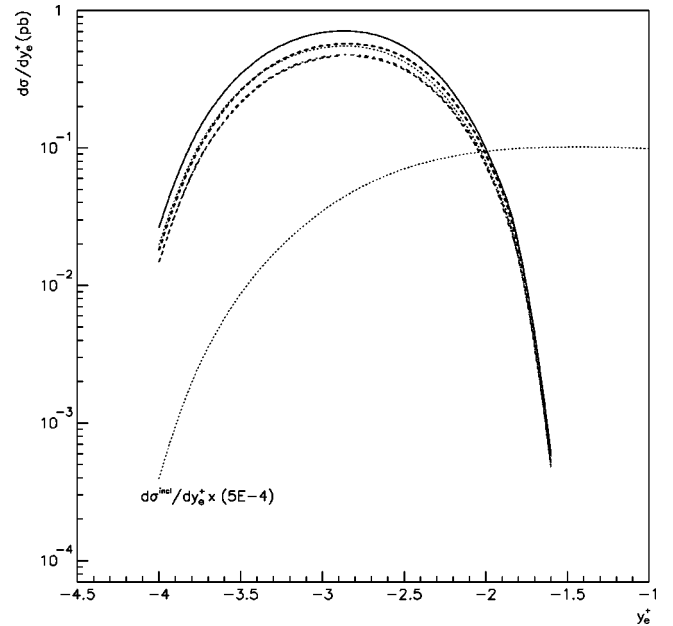

FIG. 10. Rapidity distribution of e^+ in W^+ production with the cut $x_P < 0.01$. The description of the various curves is the same as in the caption for Fig. 9.

So in Table VIII we present our diffractive fractions using Eq. (13) and our fits with $\alpha_P = 1.14$ for several different values of x_P^{max}. They are computed with the diffracted hadron being allowed to be either the proton or the antiproton. We see that for $x_P^{\text{max}} = 0.01$, the rates are an order of magnitude smaller, while for $x_P^{\text{max}} = 0.05$, the rates are of the same order as the data. However, the preferred fits, with a large amount of initial glue (B, D and SG), yield rates which are about 2–3 times larger than the data. For $x_P^{\text{max}} = 0.1$, our rates are a factor 3–6 larger than the central data value.

V. DIFFRACTIVE JETS

In this section, we present our results for jet production. We imposed the following cuts on the jet cross sections. These represent the effect of appropriate experimental cuts [14,17] and of cuts to improve the significance of the signal.

(i) We require that two jets be produced in the same half of the detector, i.e., $y_1 y_2 > 0$, where y_i is the rapidity of jet i. This eliminates the region where the jets are in opposite hemispheres, since that region is well populated by non-diffractive events but is relatively unpopulated by diffractive events, because of the rapidity gap requirement.

TABLE VIII. Diffractive fractions R_W for W production when either p or $\bar{p}$ diffracts.

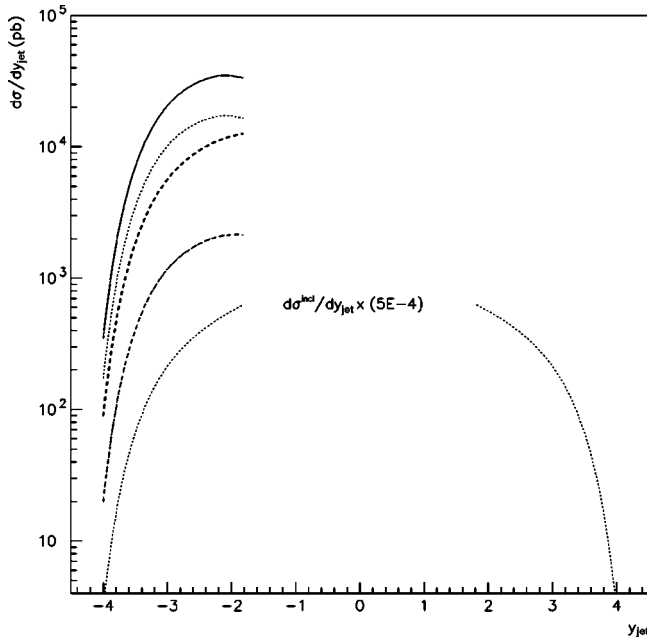| Fit	$x_P^{\text{max}} = 0.01$	$x_P^{\text{max}} = 0.05$	$x_P^{\text{max}} = 0.1$
A	0.12%	1.9%	3.3%
B	0.14%	2.6%	5.1%
C	0.12%	1.8%	3.2%
D	0.18%	3.5%	6.9%
SG	0.14%	2.2%	4.1%

FIG. 11. Rapidity distribution of jet cross sections, with $E_T > 20$ GeV, $y > 1.8$, and $x_P < 0.01$. The description of the various curves is the same as in the caption for Fig. 9.

(ii) Each jet is required to have a transverse energy E_T greater than 20 GeV. This ensures that we are definitely in the perturbative region for the jets, but the cut could be relaxed.

(iii) Each jet's rapidity satisfies $|y| > y_{cut} \equiv 1.8$.

Next, we integrated over the rapidity of one of the jets to obtain a single jet distribution, but still subject to the above cuts on the other jet. Equations (11) and (17) were used for the diffractive and inclusive cross sections, respectively, with the parton distributions evolved to the scale E_T. For the diffractive cross sections, the x_P integral was performed up to $x_P^{max} = 0.01$. In the following discussion, we will denote the rapidity of the final state jet by y_{jet} instead of y.

The resulting cross sections are shown in Fig. 11. There are no points in the middle part of the plot because of the rapidity cut. The cross sections using low glue fits A and C are nearly identical as depicted by the overlapping dashed (A) and dot-dashed (C) curves in the figure. The high glue fits D (solid curve), B (dotted curve) and SG (heavy dashed curve) yield cross sections that are about an order of magnitude larger, with D being largest, than those using low glue fits. This difference reflects the sensitivity of this particular type of cross section to the gluon content of the Pomeron. The lower dotted curve, which is symmetric about $y = 0$, represents the inclusive cross section scaled down by a factor of 5×10^{-4}.

The diffractive jet percentages are shown in Fig. 12, where $R \times 100$ is plotted as a function of y_{jet}, with

$$R = \frac{d\sigma^{jet, \ diff}/dy_{jet}}{d\sigma^{jet, \ incl}/dy_{jet}}.$$

One finds that the rates R are largest when fit D is used, varying from 2.7% to 5.7%. With fit B, whose gluon distri-
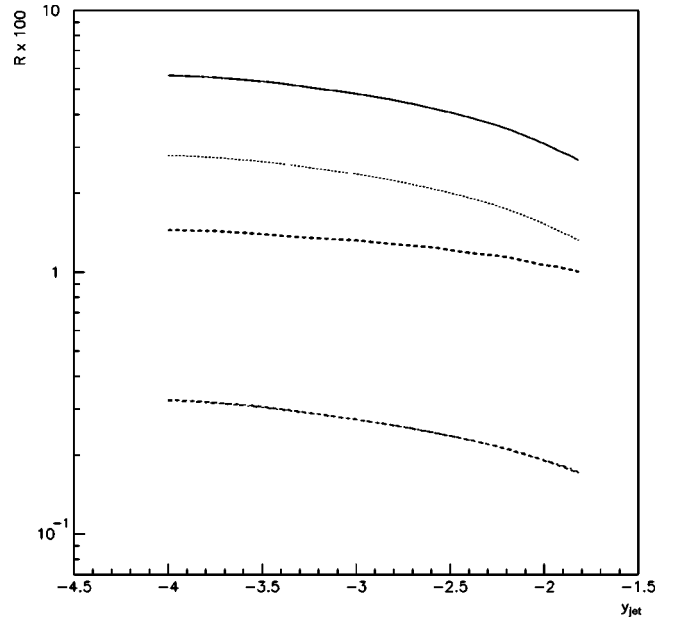

FIG. 12. Diffractive jet production percentages, with $E_T > 20$ GeV, $y > 1.8$, and $x_P < 0.01$. The solid curve results from using fit D, upper dashed curve with fit SG, dotted curve with fit B, lower dashed curve with fit A and dot-dashed curve with fit C.

bution is about a factor of 2 lower than fit D, the rates are also about a factor of 2 smaller. The rates obtained with fits A and C are much lower, ranging from 0.2% to about 0.3%. With fit SG, the resulting curve is relatively flat, giving a rate of about 1.2%. The rates are largest at $y_{jet} = -4$, then decrease as y_{jet} increases. Of course, the large rates for distributions D, B and SG, all with the large gluon distribution, directly result from the fact that there is a gluon-induced subprocess.

We end this section by making comparisons with data on diffractive dijet production from CDF and D0 at $\sqrt{s} = 1800$ GeV. CDF has measured dijet data both with a rapidity gap requirement [14] and with Roman pots [15] along the antiproton beam direction. In the first case, the cross section for dijets produced opposite a rapidity (η) gap in the region $2.4 < |\eta| < 4.2$ is measured. Each jet is required to have a minimum E_T of 20 GeV and rapidity $1.8 < |\eta| < 3.5$. They also measure the dijet cross section without a rapidity gap, i.e., what we refer to in this paper as the inclusive cross section. The diffractive fraction they measure is [14] $R_{JJ} = [0.75 \pm 0.05(\text{stat}) \pm 0.09(\text{syst})]\%$. This measured value is appropriate for $x_P \lesssim 0.1$ [35]. The fractions that we obtain using the above cuts and our fits with $\alpha_P = 1.14$ are shown in Table IX, for several values of x_P^{max}. Our calculation assumes that either the antiproton or the proton is diffracted. The rates obtained with fit D or B are from 3 to 22 times larger, while those obtained with fit C or A range from being about 70% smaller to being a few percent larger than the measured value, depending on the value of x_P^{max}. The rates using fit SG are also significantly greater than the data but smaller than the rates with fits B and D. This reflects the low number of gluons in fit SG; they were more effective in the photoproduction at producing jets be-

TABLE IX. Diffractive fractions R_{JJ} for dijet production when either p or $\bar{p}$ diffracts and using cuts on E_T and y appropriate for the CDF rapidity gap data.

Fit	$x_{\mathbb{P}}^{\max}=0.01$	$x_{\mathbb{P}}^{\max}=0.05$	$x_{\mathbb{P}}^{\max}=0.1$
A	0.23%	0.63%	0.83%
B	1.9%	6.0%	8.1%
C	0.23%	0.61%	0.79%
D	3.9%	12.3%	16.4%
SG	1.2%	2.5%	3.2%

cause of their relatively large fractional momentum relative to the Pomeron.

With their Roman-pot-triggered diffractive sample, CDF has measured a diffractive fraction of $R_{JJ}=[0.109\pm0.003 \pm0.016]\%$. The data in this sample correspond to $x_{\mathbb{P}}$ in the range $0.05<x_{\mathbb{P}}<0.1$, with the jets having minimum E_T of 10 GeV. The fractions we obtain using the same kinematic cuts and our fits with $\alpha_{\mathbb{P}}=1.14$ are presented in Table X. In this case, our calculation assumes that only the antiproton is diffracted. The ones obtained with fits D, B and SG are from 8 to 34 times larger than the data, while those obtained with fits C and A are about twice as large.

Finally, D0 also has some preliminary data [17] on diffractive dijet production. They require a rapidity gap opposite the dijets, which have $E_T^{\min}=12$ GeV and $|\eta_{\mathrm{jet}}|>1.6$. The diffractive fraction they measure with an estimated $x_{\mathbb{P}}^{\max}=0.03$ is $R_{JJ}=[0.67\pm0.05]\%$. Our calculated fractions are shown in Table XI; as with our previous calculations, we use the fits with $\alpha_{\mathbb{P}}=1.14$ and assume that either the antiproton or the proton is diffracted, The realistic fits (with a large gluon content) are well above the data, by factors of 9, 18, and 4 for fits B, D, and SG, respectively. The cross sections obtained from fits A and C are a bit smaller than the data; these fits give a correct normalization for diffractive DIS, so again we see the importance of the photoproduction data in demonstrating a breakdown of factorization.

VI. CONCLUSIONS

We have presented parton distributions in the Pomeron resulting from fits to data on diffractive DIS and diffractive photoproduction at HERA. In order to explore the sensitivity of the data to different aspects of the parton densities, we made several fits with different assumptions for the initial parton densities. We find that only those parametrizations with a large amount of glue (B, D and SG) are able to provide a good fit to the photoproduction data. The other two parametrizations (A and C), which are constrained to have no

TABLE X. Diffractive fractions R_{JJ} for dijet production when only $\bar{p}$ diffracts and using cuts on $x_{\mathbb{P}}$, E_T and y appropriate to the CDF Roman pot data.

Fit	A	B	C	D	SG
R_{JJ}	0.20%	1.8%	0.19%	3.7%	0.85%

TABLE XI. Diffractive fractions R_{JJ} for dijet production when either p or $\bar{p}$ diffracts and using cuts on $x_{\mathbb{P}}$, E_T and y appropriate for the D0 data.

Fit	A	B	C	D	SG
R_{JJ}	0.59%	5.8%	0.57%	11.8%	2.4%

gluons in the starting distributions, badly underestimate the photoproduction cross sections.

We also find that the normalizations of both the quark and gluon densities in the Pomeron are well determined by the data. As regards the shape, hard distributions are preferred. But in the case of the gluon, the question still remains as to whether a conventional hard distribution ($1-\beta$ at large β) or something harder is correct. We are able to obtain satisfactory fits with both a hard gluon, in fit D, and a harder gluon, in fit SG. We have shown how measurements of the β dependence of the photoproduction cross section will be able to provide much better information.

From our fits, we predicted the cross sections for vector boson production and dijet production in diffractive $p\bar{p}$ interactions at the Tevatron. The rates represent a realistic prediction of the cross sections, *given the assumption of factorization*. We find that the predictions are a factor of several above the measured cross sections. In the case of the jet cross sections, it is only for the physically correct ''high-gluon'' fits that the predictions substantially exceed the data. The lack of agreement between the predictions and the data indicates a substantial breakdown of factorization in diffractive $p\bar{p}$ interactions.

For the predictions to match the measured diffractive rates of W production by CDF, suppression factors ($\equiv$ prediction/ data) ranging from 3 to 6 must be applied. In the case of diffractive dijet production, the suppression factors appear to be somewhat larger, around 10. (We refer only to the realistic fits, with a large amount of glue.)

Further work to measure the suppression factors is necessary to obtain a fuller understanding of the dynamics of diffractive hadron-hadron interactions. One interesting possibility is to search for the contribution predicted by the coherent Pomeron mechanism of Collins, Frankfurt and Strikman [1], which in fact gives an *enhancement* of the cross section at large β. Such an enhancement is suggested by the UA8 data [11]. This and our results on photoproduction show that the measurement of β distributions is important. It should be noted that the UA8 data are at larger $|t|$ than the data which we have fitted.

With regards to extracting diffractive parton densities, further work is also needed to understand the differences between the ZEUS and H1 data, as illustrated in Fig. 6. The differences are suggestive of a systematic error that is correlated point-to-point. This indicates that we need to be careful about taking the χ^2 values at face value, and in fact that systematic errors need to be treated more correctly. Our negative value for the soft quark term in fit D is worrying; note that it is driven by the H1 data, as can be seen from the χ^2 values in Table II.

It is also important to test the universality of α_{P}, for example, to test whether its value is different in exclusive and inclusive processes, as is suggested by Fig. 7.

Finally, further tests of factorization can be accomplished at HERA. For example, we expect hard-scattering factorization to be valid for heavy quark production in DIS as well, but not for any resolved photoproduction process.

Note added. After completion of the work for this paper, a paper by the ZEUS Collaboration [36] appeared. It provides the official version of the diffractive photoproduction data [25] that we showed in Fig. 8, and the paper reports a QCD analysis of the ZEUS data. This analysis was performed in-dependently of the one in the present paper, but in a similar style, and the conclusions as regards the parton densities in the Pomeron are similar.

[1] J.C. Collins, L. Frankfurt, and M. Strikman, Phys. Lett. B **307**, 161 (1993); A. Berera and J.C. Collins, Nucl. Phys. **B474**, 183 (1996).

[2] P.V. Landshoff and J.C. Polkinghorne, Nucl. Phys. **B33**, 221 (1971); **B36**, 642 (1972); F. Henyey and R. Savit, Phys. Lett. **52B**, 71 (1974); J.L. Cardy and G.A. Winbow, *ibid.* **52B**, 95 (1974); C. DeTar, S.D. Ellis, and P.V. Landshoff, Nucl. Phys. **B87**, 176 (1975).

[3] G. Ingelman and P.E. Schlein, Phys. Lett. **152B**, 256 (1985).

[4] J.C. Collins, J. Huston, J. Pumplin, H. Weerts, and J.J. Whitmore, Phys. Rev. D **51**, 3182 (1995).

[5] L. Alvero, J.C. Collins, J. Terron, and J. Whitmore, hep-ph/9701374.

[6] ZEUS Collaboration, M. Derrick *et al.*, Z. Phys. C **68**, 569 (1995); ZEUS Collaboration, M. Derrick *et al.*, *ibid.* **70**, 391 (1996).

[7] ZEUS Collaboration, J. Breitweg *et al.*, Eur. Phys. J. C **1**, 81 (1998).

[8] H1 Collaboration, C. Adloff *et al.*, Z. Phys. C **76**, 613 (1997).

[9] ZEUS Collaboration, M. Derrick *et al.*, Phys. Lett. B **356**, 129 (1995).

[10] ZEUS Collaboration, M. Derrick *et al.*, Phys. Lett. B **315**, 481 (1993); **332**, 228 (1994); H1 Collaboration, T. Ahmed *et al.*, Nucl. Phys. **B429**, 477 (1994).

[11] UA8 Collaboration, A. Brandt *et al.*, Phys. Lett. B **297**, 417 (1992).

[12] UA1 Collaboration, K. Eggert, in *Elastic and Diffractive Scattering*, edited by K. Goulianos (Editions Frontières, Gif-sur-Yvette, France, 1988).

[13] CDF Collaboration, F. Abe *et al.*, Phys. Rev. Lett. **78**, 2698 (1997).

[14] CDF Collaboration, F. Abe *et al.*, Phys. Rev. Lett. **79**, 2636 (1997).

[15] CDF Collaboration, P.L. Mélèse, ''Diffractive Dijet Search with Roman Pots at CDF,'' Report No. Fermilab-Conf-96/231-E.

[16] D0 Collaboration, K. Mauritz, ''Hard Diffraction at D0,'' presented at Small *x* Meeting, Argonne, IL, 1996.

[17] D0 Collaboration, S. Abachi, ''Hard Single Diffractive Jet Production at D0,'' Report No. Fermilab-Conf-96/247-E.

[18] D0 Collaboration, A.G. Brandt, ''Rapidity Gaps in Jet Events at D0,'' Report No. Fermilab-Conf-96/185-E.

[19] K. Goulianos, talk given at Frontiers in Strong Interactions - 6th International Conference on Elastic and Diffractive Scattering, Blois, France, 1995, hep-ph/9512291; K. Goulianos, Phys. Lett. B **358**, 379 (1995).

[20] J.C. Collins, Phys. Rev. D **57**, 3051 (1998).

[21] Z. Kunszt and W.J. Stirling, in *Deep Inelastic Scattering and Related Phenomena (DIS-96)*, edited by G. D'Agostini and A. Nigro (World Scientific, Singapore 1997), hep-ph/9609245.

[22] A. Berera and D.E. Soper, Phys. Rev. D **50**, 4328 (1994).

[23] A. Berera and D.E. Soper, Phys. Rev. D **53**, 6162 (1996).

[24] Yu. L. Dokshitzer, at the HEP EPS Conference, Jerusalem, 1997, hep-ph/9801372.

[25] ZEUS Collaboration, ''Diffractive Dijet Cross Sections and Rapidity Gap Between Jets in Hard Photoproduction at HERA,'' Report No. N-648/N-655, contribution to EPS97, Jerusalem, 1997, http://www-zeus.desy.de/plots97/eps97/et_difdijF.ps.

[26] L. Alvero and J.C. Collins, POMPYT-S.C.: A Modified version of POMPYT to use evolved parton densities, ftp:// ftp.phys.psu.edu/pub/hep-tools/pompyt.

[27] P. Bruni and G. Ingelman, Phys. Lett. B **311**, 317 (1993).

[28] T. Gehrmann and W.J. Stirling, Z. Phys. C **70**, 89 (1996).

[29] K. Golec-Biernat and J. Kwieciński, Phys. Lett. B **353**, 329 (1995).

[30] A. Donnachie and P.V. Landshoff, Phys. Lett. B **191**, 309 (1987); Nucl. Phys. **B303**, 634 (1988).

[31] The CTEQ evolution package is part of the POMPYT-S.C. package [26].

[32] E. Eichten, I. Hinchliffe, K. Lane, and C. Quigg, Rev. Mod. Phys. **56**, 579 (1984); **58**, 1065 (1986).

[33] R. Hamberg, W.L. van Neerven, and T. Matsuura, Nucl. Phys. **B359**, 343 (1991).

[34] Particle Data Group, R.M. Barnett *et al.*, Phys. Rev. D **54**, 1 (1996).

[35] CDF Collaboration, K. Goulianos, in Proceedings of the XXXIInd Rencontre de Moriond, ''′97 QCD and High Energy Hadronic Interactions,'' edited by J. Tran Thanh Van (Editions Frontières, Gif-sur-Yvette, France, 1997), p. 447.

[36] ZEUS Collaboration, J. Breitweg *et al.*, Eur. Phys. J. C **5**, 41 (1998).